



Temporal variations of flux and altitude of volcanic sulfur dioxide emissions

M. Boichu et al.

This discussion paper is/has been under review for the journal Atmospheric Chemistry and Physics (ACP). Please refer to the corresponding final paper in ACP if available.

Temporal variations of flux and altitude of sulfur dioxide emissions during volcanic eruptions: implications for long-range dispersal of volcanic clouds

M. Boichu¹, L. Clarisse², J.-C. Péré¹, H. Herbin¹, P. Goloub¹, F. Thieuleux¹, F. Ducos¹, C. Clerbaux^{2,3}, and D. Tanré¹

¹Laboratoire d'Optique Atmosphérique, Université Lille 1, UMR8518 CNRS, Villeneuve d'Ascq, France

²Spectroscopie de l'Atmosphère, Service de Chimie Quantique et Photophysique, Université Libre de Bruxelles, Brussels, Belgium

³Sorbonne Universités, UPMC Univ. Paris 06; Université Versailles St-Quentin; CNRS/INSU, LATMOS-IPSL, Paris, France

Received: 18 December 2014 – Accepted: 6 February 2015 – Published: 23 February 2015

Correspondence to: M. Boichu (marie.boichu@univ-lille1.fr)

Published by Copernicus Publications on behalf of the European Geosciences Union.

Title Page

Abstract

Introduction

Conclusions

References

Tables

Figures



Back

Close

Full Screen / Esc

Printer-friendly Version

Interactive Discussion



Abstract

Sulfur-rich degassing, which is mostly composed of sulfur dioxide (SO_2), plays a major role in the overall impact of volcanism on the atmosphere and climate. The accurate assessment of this impact is currently hampered by the poor knowledge of volcanic SO_2 emissions. Here, using an inversion procedure, we show how assimilating snapshots of the volcanic SO_2 load derived from the Infrared Atmospheric Sounding Interferometer (IASI) allows for reconstructing both the flux and altitude of the SO_2 emissions with an hourly resolution. For this purpose, the regional chemistry-transport model CHIMERE is used to describe the dispersion of SO_2 when released in the atmosphere. As proof of concept, we study the 10 April 2011 eruption of the Etna volcano (Italy), which represents one of the few volcanoes instrumented on the ground for the continuous monitoring of SO_2 degassing.

We find that the SO_2 flux time-series retrieved from satellite imagery using the inverse scheme is in agreement with ground observations during ash-poor phases of the eruption. However, large discrepancies are observed during the ash-rich paroxysmal phase as a result of enhanced plume opacity affecting ground-based ultraviolet (UV) spectroscopic retrievals. As a consequence, the SO_2 emission rate derived from the ground is underestimated by almost one order of magnitude.

Altitudes of the SO_2 emissions predicted by the inverse scheme are validated against a RGB MODIS image capturing the near-source atmospheric pathways followed by Etna plumes, in combination with forward trajectories from the Hybrid Single Particle Lagrangian Integrated Trajectory (HYSPLIT) model. At large distance from the source, modeled SO_2 altitudes are confronted with independent information on the volcanic cloud height. We find that the altitude predicted by the inverse scheme is in agreement with snapshots of the SO_2 height retrieved from recent algorithms exploiting the high spectral resolution of IASI. The validity of the modeled SO_2 altitude is further confirmed by the detection of a layer of particles at the same altitude by the spaceborne CALIOP

ACPD

15, 5031–5077, 2015

Temporal variations of flux and altitude of volcanic sulfur dioxide emissions

M. Boichu et al.

Title Page

Abstract

Introduction

Conclusions

References

Tables

Figures



Back

Close

Full Screen / Esc

Printer-friendly Version

Interactive Discussion



LiDAR. Analysis of CALIOP color and depolarization ratios suggests that these particles consist of sulfate aerosols formed from precursory volcanic SO₂.

The reconstruction of emission altitude, through inversion procedures which assimilate volcanic SO₂ column amounts, requires specific meteorological conditions, especially sufficient wind shear so that gas parcels emitted at different altitudes follow distinct trajectories. We consequently explore the possibility and limits of assimilating in inverse schemes infrared (IR) imagery of the volcanic SO₂ cloud altitude which will render the inversion procedure independent of the wind shear prerequisite.

1 Introduction

Among the various gaseous compounds released by volcanoes, sulfur emissions are of major concern as they exert a fundamental role on the atmosphere and climate (Oppenheimer et al., 2011). The impact on climate of major eruptions, which emit sulfur-rich gases (and mainly sulfur dioxide (SO₂)) directly into the stratosphere, has long been recognized (McCormick et al., 1995). In addition to major eruptions, more frequent intermediate-size eruptions impacting the lower stratosphere have also been pointed out as a possible cause of the recent pause in the global warming trend (Vernier et al., 2011; Solomon et al., 2011; Neely et al., 2013; Santer et al., 2013, 2014). Secondary sulfate aerosols, which result from the oxidation of sulfur gases in the atmosphere, are the main protagonists of this volcanic forcing. Micron-size sulfate aerosols, whose lifetime may reach a few years in the stratosphere, are capable of scattering solar radiation and cause transient cooling of the atmosphere from regional to global scales (Robock, 2000). They may also catalyze the destruction of stratospheric ozone (Solomon, 1999).

In contrast, less powerful tropospheric eruptions are generally considered harmless in terms of climatic impact. Indeed, in the troposphere, aerosols are rapidly washed out by precipitations and have a short lifetime (Stevenson et al., 2003). However, sulfate aerosols may reduce ice crystal nucleation rate and impact the properties of high

Temporal variations of flux and altitude of volcanic sulfur dioxide emissions

M. Boichu et al.

Title Page

Abstract

Introduction

Conclusions

References

Tables

Figures



Back

Close

Full Screen / Esc

Printer-friendly Version

Interactive Discussion



from the source are confronted with our predictions. SO₂ altitudes derived directly from IASI images allow for assessing the potential bias between our inversion results on one hand and the IASI advanced algorithm on the other. Detection of the volcanic cloud captured by a track of the spaceborne CALIOP LiDAR is also compared to our estimated altitude. The potential implications in terms of a simultaneous retrieval of SO₂ gas and sulfate aerosol components in volcanic clouds are discussed in light of the latter comparison.

2 Methodology

2.1 Inversion procedure

2.1.1 Chemistry-transport model

The atmospheric dispersal of the volcanic cloud is described using the CHIMERE regional Eulerian chemistry-transport model (CTM) (Boichu et al., 2013, 2014; Menut et al., 2013). The model accounts for various physico-chemical processes affecting the SO₂ released in the atmosphere, including transport, turbulent mixing, diffusion, dry deposition, wet scavenging and gas/aqueous-phase chemistry. However, the conversion of SO₂ to sulfate aerosols is not implemented in this study due to uncertainty on the numerous factors controlling this process in a volcanic context. CHIMERE CTM is driven by meteorological fields from the Weather Research and Forecasting (WRF) model (Skamarock et al., 2008), which is forced by NCEP (National Centers for Environmental Prediction) reanalysis data on a six hour basis. WRF meteorological fields have a 20 km × 20 km horizontal grid and 30 hybrid sigma-pressure vertical layers extending up to ~ 19 km. CHIMERE CTM has the same horizontal resolution (20 km × 20 km) but a finer vertical resolution with 29 hybrid sigma-pressure vertical layers extending up to 150 hPa (~ 13 km a.s.l.). SO₂ emissions are released along a Gaussian profile centered at a specific height with a full width at half maximum of 100 m.

Temporal variations of flux and altitude of volcanic sulfur dioxide emissions

M. Boichu et al.

Title Page

Abstract

Introduction

Conclusions

References

Tables

Figures

◀

▶

◀

▶

Back

Close

Full Screen / Esc

Printer-friendly Version

Interactive Discussion



2.1.2 Observations

SO₂ column amount maps were retrieved from measurements of the Infrared Atmospheric Sounding Interferometer (IASI) carried on board the polar-orbiting MetOp-A satellite (Clerbaux et al., 2009). Since 2007, global coverage has been provided twice a day (mean overpass times at ~ 09:30 and 21:30 local time at the Equator) with a pixel footprint of 12 km diameter (at nadir) and full swath width of 2200 km. The Fourier transform spectrometer spans a spectral range from 645 to 2760 cm⁻¹ with no gaps, an apodised resolution of 0.5 cm⁻¹ and a sampling of 0.25 cm⁻¹. It covers three bands of SO₂ absorption in the mid-infrared (Clarisse et al., 2012). Here, a series of four SO₂ column amount maps (10 April 2011 a.m. and p.m., 11 April a.m. and p.m.) was calculated using the algorithm of Clarisse et al. (2014). After the retrieval of the SO₂ altitude, which is described in Sect. 2.2.2, an optimal estimation scheme with generalized noise covariance, similar to the one of Carboni et al. (2012), is used for SO₂ column retrieval.

2.1.3 Inversion settings

The inversion procedure aims at reconstructing the temporal variations of both the flux and the altitude of volcanic SO₂ emissions with an hourly resolution. The inverse scheme uses satellite observations of SO₂ column amounts in combination with a chemistry-transport model as a forward model (Boichu et al., 2013, 2014). The inverse problem is solved by determining the time history of SO₂ emissions, in terms of flux and altitude, that minimizes (in the least squares sense) the misfit between observed and modeled spatial and temporal distributions of SO₂ for the series of four IASI images of the SO₂ cloud (10 April a.m. and p.m., 11 April a.m. and p.m.).

The inversion procedure developed by Boichu et al. (2013, 2014) used information on the altitude of SO₂ emission from independent radar ground observations to reconstruct flux emissions. Here, the algorithm extends this procedure by considering the altitude as an additional source parameter to reconstruct. Except for a nonnegative

Temporal variations of flux and altitude of volcanic sulfur dioxide emissions

M. Boichu et al.

Title Page

Abstract

Introduction

Conclusions

References

Tables

Figures



Back

Close

Full Screen / Esc

Printer-friendly Version

Interactive Discussion



constraint on flux values, no a priori knowledge on SO₂ flux and emission altitude is required in this inversion procedure. However, in order to retain a reasonable number of parameters, we conducted preliminary tests with nine candidate emission altitudes, ranging from 4 km to 12 km a.s.l., with a spacing of 1 km. The lowest altitude is just above the altitude of Etna, which culminates at 3.4 km a.s.l. Results showed that the best fit to observations is reached with only two emission altitudes at 4 and 7 km a.s.l. Considering more than two altitudes marginally improves the fit.

A smoothing scheme is applied on the variations of flux with time only (i.e. no smoothing is applied across different altitude bins). The amount of smoothing is adjusted by a single meta-parameter in the inversion. Figure 1 shows how the misfit to observations increases significantly for roughness values < 0.56 th⁻³. However, as underlined by the logarithmic scale for roughness axis in Fig. 1, the misfit remains almost constant for roughness exceeding 0.56 th⁻³, which is consequently chosen as the optimal roughness in our inversion scheme. The set of pixels corresponding to a mass load below the detection threshold (null detection) is decimated by a factor 3 to both tackle numerical diffusion biases and attribute less weight to null detection in the inverse scheme, as null detection may correspond to low SO₂ concentrations in reality (Boichu et al., 2013).

2.2 Products used for validation

2.2.1 Ground observations

A network of nine ultraviolet (UV) spectrometers has been scanning continuously the sky of Mt. Etna since 2005 (Salerno et al., 2009). On 10 April 2011, three out of the nine spectrometers of the network intersected Etna's plume at a distance of ~ 14 km from the summit craters (Bonaccorso et al., 2011). If UV radiation received by these instruments is sufficient (i.e. during daylight hours, under favorable meteorological conditions and during eruptive periods emitting an optically thin volcanic plume), such a network allows for monitoring the SO₂ flux emitted by the volcano with a temporal resolution of

Temporal variations of flux and altitude of volcanic sulfur dioxide emissions

M. Boichu et al.

Title Page

Abstract

Introduction

Conclusions

References

Tables

Figures



Back

Close

Full Screen / Esc

Printer-friendly Version

Interactive Discussion



~ 6 min. Hence, on 10 April 2011, Etna SO₂ emission rates could be measured from 7 a.m. to 3 p.m. (Bonaccorso et al., 2011) allowing for capturing the 10 April eruptive episode which, fortunately, occurred mostly during daylight hours.

A permanent network of 32 broadband seismic stations is installed on Mt. Etna. The network is designed to monitor the temporal evolution of the seismic tremor, which is continuous at Etna, and is closely related to variations of the volcanic activity. Of interest here is to explore the root mean square (RMS) amplitude of the seismic tremor (smoothed on a 5 min-long sliding window in the frequency band 0.5–5 Hz) recorded at the EBEL station, which is the closest station to the South-East Crater (SEC) where the lava fountain activity took place on 10 April.

2.2.2 Satellite observations

The altitude of the SO₂ cloud is retrieved from IASI observations using the algorithm outlined in Clarisse et al. (2014), which estimates the altitude independently from the column. Here we summarize the main features of the algorithm and refer to the aforementioned study for full details. Central is the use of a response function, which, simply put, is a weighted projection of the observed spectrum onto different Jacobians. These Jacobians are derived by perturbing a representative background atmosphere with small amounts of SO₂ at different altitudes. The retrieved altitude corresponds to that altitude for which the response function reaches its maximum.

This algorithm does not rely on any a priori information on the altitude. This is an appealing feature, as all of the extracted information comes directly from the observed spectrum, and is not being weighted with a priori information. However, for very small SO₂ spectral signatures, this also means that the algorithm can return unrealistic altitudes (typically, either very high or very low altitude values). These outlier values are usually found at the plume edges. The second peculiarity of this algorithm is that it does not rely on an inverse model, nor on iterative fitting. Calculation of the response function is almost instantaneous, and this makes the algorithm highly suitable for Near Real Time (NRT) applications. However, the use of a constant background atmosphere can

Temporal variations of flux and altitude of volcanic sulfur dioxide emissions

M. Boichu et al.

Title Page

Abstract

Introduction

Conclusions

References

Tables

Figures



Back

Close

Full Screen / Esc

Printer-friendly Version

Interactive Discussion



introduce a bias on the retrieved altitudes. This is especially the case if the background water vapor atmospheric profile differs significantly from the real one.

Two Etna plumes leaving Sicily could be RGB-imaged on 10 April 2011 (12:30 UT) using Level 1B radiances at three spectral bands (459–479, 545–565 and 620–670 nm) of the MODerate Resolution Imaging Spectroradiometer (MODIS) carried on-board the polar orbiting AQUA satellite. Radiances are provided with a resolution of 250 m at nadir. Visible channels are rarely used for volcanic applications due to the difficulty of unambiguously discriminating volcanic clouds from other types of aerosols (Zakšek et al., 2013), compared to the IR channels widely exploited for ash remote sensing (Watson et al., 2004; Prata, 2009; Dubuisson et al., 2014). Here, the blue channel was stretched in order to outline the presence of a thinner plume which would otherwise remain invisible.

A vertically resolved profile of the distant volcanic cloud of Etna was acquired with the Cloud-Aerosol LiDAR with Orthogonal Polarization (CALIOP), carried onboard the CALIPSO satellite, which is an elastic backscatter LiDAR operating at 532 and 1064 nm. CALIOP LiDAR observations have been used to track the vertical distribution of volcanic clouds from stratospheric (Haywood et al., 2010) but also tropospheric (Winker et al., 2012; Vernier et al., 2011) eruptions of moderate intensity. The Etna eruption studied here is of lower magnitude than eruptions previously studied using CALIOP observations. Given the age of the volcanic cloud at the time of intersection with the CALIOP track (already 12 h-old according to the dispersal model), we consequently expect to detect a relatively thin layer of aerosols. However, we take advantage of a night track (00:26 UT on 11 April 2011) which favors a higher signal to noise ratio for the Level 1 total attenuated backscatter signal at 532 nm. This allows for detecting the tenuous aged Etna cloud. Information on the altitude, the color ratio (defined as the ratio of particulate backscatter coefficients at 1064 and 532 nm) and the depolarization ratios (volume and particulate) of both aerosol and cloud layers from CALIOP Level 2 products are used to discriminate the volcanic cloud from surrounding upper-tropospheric meteorological clouds.

Temporal variations of flux and altitude of volcanic sulfur dioxide emissions

M. Boichu et al.

Title Page

Abstract

Introduction

Conclusions

References

Tables

Figures



Back

Close

Full Screen / Esc

Printer-friendly Version

Interactive Discussion



The fraction of meteorological clouds present at a given IASI pixel is estimated using the Cloud Cover Factor (CCF) from EUMETSAT IASI Level 2 products (August et al., 2012).

2.2.3 Trajectory model

The Hybrid Single Particle Lagrangian Integrated Trajectory (HYSPLIT) model of the Air Resources Laboratory of the National Oceanic and Atmospheric Administration (NOAA) is used to compute air parcel trajectories (Draxler and Rolph, 2014). For our application to Etna, both forward and backward trajectories are calculated with HYSPLIT which is driven by NCEP/GDAS (Global Data Assimilation System) 3-hourly meteorological reanalysis with a latitude/longitude resolution of $1^\circ \times 1^\circ$ and 23 vertical layers up to 20 hPa.

3 Results and validation

3.1 SO₂ flux emissions: ground versus satellite

A series of four IASI SO₂ column amount maps (Fig. 2 left) are used for constraining the reconstruction of both flux and altitude of Etna's emissions by inverse modeling (histograms in Top of Fig. 3). On the first map (Fig. 2a left), a few pixels indicate the presence of SO₂ close to Etna on 10 April at around 08:00 UT¹, which supports an eruption start before this time. The assimilation of these acquisitions in the inverse scheme dates the first release of SO₂ between 05:00 and 07:00 UT, with a low flux of $\sim 50 \text{ th}^{-1}$. So early, UV radiation is insufficient for ground UV-spectrometers to operate (top of Fig. 3, green line).

Acquisition of the second image around 20:00 on 10 April highlights a large SO₂ cloud with a complex horseshoe shape, which could suggest the existence of significant

¹All times are UT (Universal Time), unless otherwise specified.

Temporal variations of flux and altitude of volcanic sulfur dioxide emissions

M. Boichu et al.

Title Page

Abstract

Introduction

Conclusions

References

Tables

Figures



Back

Close

Full Screen / Esc

Printer-friendly Version

Interactive Discussion



Temporal variations of flux and altitude of volcanic sulfur dioxide emissions

M. Boichu et al.

Title Page

Abstract

Introduction

Conclusions

References

Tables

Figures

◀

▶

◀

▶

Back

Close

Full Screen / Esc

Printer-friendly Version

Interactive Discussion



emissions start to be released (Bonaccorso et al., 2011) (grey area in Fig. 3), which reveals the increasing degree of explosivity of the eruption and the occurrence of magma fragmentation triggering ash discharge. The comparison between ground and satellite-derived fluxes therefore indicates a good agreement during ash-poor periods of the Etna eruption. In contrast, the increasing plume opacity associated to the abundance of ash likely leads to an underestimation of SO₂ emission rates derived from ground measurements, reaching almost an order of magnitude (a factor 8 here), during the ash-rich paroxysmal phase of the eruption.

The existence of significant wind shear is confirmed by IASI acquisitions on 11 April at ~ 08:00 and 18:30, which indicate a large elongation and dispersion of the SO₂ cloud (Fig. 2c and d left). The SO₂ cloud covers now more than 1200 km, only 12 h since the previous observations that indicated a much more spatially concentrated SO₂ cloud (Fig. 2b left). The model is able to reproduce the SO₂ cloud elongation as well as the gradients of SO₂ load within the plume (Fig. 2c and d right). Nevertheless, we observe a discrepancy between observations and model at these dates. The observed SO₂ cloud appears extremely narrow which is in disagreement with the model. Numerical diffusion may induce more spreading of the modelled volcanic cloud than observed. Also, in case of a lower SO₂ load, the presence of thick meteorological clouds close to the core of the plume on 11 April a.m. and p.m. maps, which is illustrated by the cloud cover fraction from Eumetsat IASI Level 2 products, can hamper the detection of SO₂, leading to artifactual gaps in observations (Fig. 4c and d).

3.2 Altitude of emissions and near-source SO₂ cloud

IASI acquisitions and model show a relatively compact SO₂ cloud composed of two linked pieces on 10 April p.m. (Fig. 2b). In contrast, subsequent maps indicate a torn apart, elongated plume (Fig. 2c and d). This behavior demonstrates the existence of an intense wind shear in the meteorological fields leading to very different trajectories followed by parts of the SO₂ cloud initially originating from a single location. Such an example illustrates the necessity and importance of rigorously accounting for the

3.3 Far-range altitude of the SO₂ cloud

3.3.1 IASI SO₂ altitude

IASI column amounts were used in the inversion procedure to reconstruct the rate and altitude of SO₂ emissions. We compare here the altitude of the dispersed Etna SO₂ cloud predicted by the model (Fig. 6 right) against the SO₂ height retrieved independently using recently developed algorithms exploiting the high spectral resolution of IASI observations (Clarisse et al., 2014) (Fig. 6 left). At a given pixel, the modeled altitude corresponds to the altitude at the middle of the layer with a maximal SO₂ concentration.

Overall, we observe an agreement between modeled and observed altitudes which follow the same trend within the volcanic cloud. Whereas the Etna SO₂ cloud on 10 April p.m. presents a relatively compact shape, we observe that it covers a broad range of altitudes (Fig. 6b). These variations likely result from the rapid variations of the altitude of emission with time (Fig. 3). The Western part of the horseshoe shape lies at an altitude between 4 and 6 km a.s.l. according to model and observations. The Eastern part reaches an altitude of up to 9 km with the model while IASI indicates altitudes up to 12 km. The two parcels undergo an intense wind shear over this range of altitudes, explaining their very different trajectories. This fuels a substantial elongation of the SO₂ cloud, with ending parts lying at drastically different altitudes. This feature is well described by model and observations (Fig. 6c and d). Nevertheless, apart from isolated points with a very high altitude above 11 km, IASI always detects the Eastern part of the SO₂ cloud a few kilometers higher than the model. These outlier values likely correspond to noisy spectra, often at the edge of the volcanic cloud, with a too weak SO₂ signature to extract any information from them.

Temporal variations of flux and altitude of volcanic sulfur dioxide emissions

M. Boichu et al.

Title Page

Abstract

Introduction

Conclusions

References

Tables

Figures



Back

Close

Full Screen / Esc

Printer-friendly Version

Interactive Discussion



3.3.2 HYSPLIT backward trajectories

The modeled altitude of the far-range SO₂ cloud is also compared with the results obtained from HYSPLIT backward trajectories (Fig. 7). On 11 April at 08:00 UT, the modeled SO₂ cloud (colocated in time and space with IASI observations, Fig. 6c) is significantly elongated (top of Fig. 7). This date is chosen for comparison with HYSPLIT as it allows us to select parts of the volcanic cloud that are geographically distant from each others, which reduces the uncertainty in HYSPLIT outputs.

HYSPLIT indicates that the trajectories initiated at the front of the SO₂ cloud, which has almost reached the South-East corner of the Mediterranean Sea, have to start at an altitude between 7 and 8 km a.s.l. to reach Etna in backward mode (bottom right of Fig. 7). This range of altitudes for the SO₂ front is in agreement with the modeled altitude between 7 and 8.5 km. HYSPLIT trajectories initiated at the tail of the SO₂ cloud, above Lybia, have to start at an altitude between 4 and 5 km a.s.l. to reach back the Etna (bottom left of Fig. 7). This is also in agreement with modeled altitudes between 4 and 5.5 km.

3.3.3 CALIOP spaceborne LiDAR observations

A single track of the CALIOP LiDAR encountered the Etna volcanic cloud, on 11 April at about 00:26 UT. Spaceborne LiDAR observations do not directly measure gaseous SO₂ but can detect aerosols of various type within the volcanic cloud, either sulfate aerosols or ash (Winker et al., 2012; Vernier et al., 2011). Nevertheless, sulfate aerosols, which are produced by conversion of the gaseous SO₂ precursor during its transit in the atmosphere, may co-exist with SO₂ within the volcanic cloud. This co-existence is confirmed here by the exploration of the Level 1 and Level 2 CALIOP products and allows us to validate the modelled SO₂ cloud altitude by independent observations.

Our model, based on the assimilation of IASI SO₂ column amounts, predicts a SO₂ cloud at an altitude between 6.4 and 7.5 km a.s.l. at the location and time of the CALIOP

Temporal variations of flux and altitude of volcanic sulfur dioxide emissions

M. Boichu et al.

[Title Page](#)[Abstract](#)[Introduction](#)[Conclusions](#)[References](#)[Tables](#)[Figures](#)[Back](#)[Close](#)[Full Screen / Esc](#)[Printer-friendly Version](#)[Interactive Discussion](#)

we note a particle depolarization ratio (0.09) slightly larger than the very low volume depolarization ratio (0.025) for these aerosols, which may indicate a small component of non-sphericity (CALIPSO Science Team and Lidar Science Working Group, 2010).

According to color and depolarization ratios, these aerosols are fine and rather spherical in shape. As a consequence, they likely correspond to sulfate aerosols. The slight component of non-sphericity might suggest that these aerosols, which travel at the same altitude as neighbor cirrus clouds, could play the role of ice nuclei and represent partially crystallized sulfuric acid droplets (Sassen et al., 1989). As ash particles were emitted during this eruption of Etna (Bonaccorso et al., 2011), we cannot entirely exclude the existence of very fine ash particles, which have not yet settled down, and may present a more spherical shape than expected due to their coating by sulfate aerosols.

4 Discussion

4.1 Complementarity with ground- and space-based ultraviolet observations

Results presented in Sect. 3.1 demonstrate that methods based on satellite imagery are capable of constraining the temporal evolution of large SO₂ fluxes emitted by volcanoes during paroxysmal eruptive phases. On the other hand, ground measurements are less likely to succeed in such conditions, as previously illustrated by the 2010 eruption of Mt. Merapi (Indonesia) (Surono et al., 2012).

Indeed, large gas emissions are generally concomittant with abundant ash discharge. When a gas-rich magma rises in the crust toward the surface, magma pressure decreases, favoring volatile exsolution and gas bubble nucleation (Oppenheimer, 2003). Further decompression fuels the growth of these gas bubbles. When bubbles are expected to occupy a large volume of the erupting mixture exceeding the threshold of 70–80 %, magma fragmentation takes place (Cashman et al., 2000). Violently

Temporal variations of flux and altitude of volcanic sulfur dioxide emissions

M. Boichu et al.

Title Page

Abstract

Introduction

Conclusions

References

Tables

Figures



Back

Close

Full Screen / Esc

Printer-friendly Version

Interactive Discussion



expanding bubbles tear the magma apart into fragments which are ejected into the atmosphere, where they solidify into ash particles.

The significant plume opacity associated to the abundance of ash may explain the underestimation of the SO₂ flux (by a factor of up to 8 here at Etna) by ground UV-DOAS observations during ash-rich phases of the eruption relatively to flux values reconstructed from satellite IR observations. Kern et al. (2012) pointed out the significant underestimation (up to 90 %) of SO₂ emission rates for high SO₂ column density plumes with conventional DOAS (Differential Optical Absorption Spectroscopy) retrieval of ground UV observations which do not take into account a realistic radiative transfer. Plume opacity associated to abundant ash load is expected to be greater than the opacity of high SO₂ density plumes.

Accordingly, infrared IASI spaceborne observations are also sensitive to the presence of ash. However, the influence of ash presented here is minimized by the use of the ν_3 band of SO₂ for its retrievals. This band around 7.4 μm , lies well outside the 8–12 μm spectral window where ash has its largest impact. Despite this, it is known that very heavy ash loadings can affect also the ν_3 band (Clarisse et al., 2012). While the IASI retrieval algorithm which has been employed here has not been investigated yet for the effects of such thick ash clouds, an inspection of the spectra on 10 April, revealed almost no detectable ash. Ash emissions may likely consist in mainly coarse particles which have already settled down at the time of IASI overpass. Possible impact of ash on the SO₂ IR retrievals can therefore be excluded for this event. This property of IR observations is fundamental to counterbalance the weaknesses of UV sensors. In addition, thermal IR channels also allow for delivering images of the SO₂ cloud over night, which brings more information on the volcanic cloud dispersal compared to UV observations acquired only during daylight hours.

Nevertheless, the complementarity of IR and UV sensors should not be overlooked. Although UV-spaceborne acquisitions from sensors like the Ozone Monitoring Instrument (OMI) are less frequent, they have the advantage of imaging SO₂ clouds in very humid conditions and at low altitude (i.e. below 5 km) (Carn et al., 2008; Surono et al.,

Temporal variations of flux and altitude of volcanic sulfur dioxide emissions

M. Boichu et al.

Title Page

Abstract

Introduction

Conclusions

References

Tables

Figures



Back

Close

Full Screen / Esc

Printer-friendly Version

Interactive Discussion



**Temporal variations
of flux and altitude of
volcanic sulfur
dioxide emissions**

M. Boichu et al.

Title Page

Abstract

Introduction

Conclusions

References

Tables

Figures



Back

Close

Full Screen / Esc

Printer-friendly Version

Interactive Discussion



2012; McCormick et al., 2013). For its part, IR IASI sensor requires relatively dry conditions and a large thermal contrast between the ground and the air (like in Siberia), to gain sufficient sensitivity for the monitoring of SO₂ emissions in the boundary layer (Bauduin et al., 2014). In the near future, the assimilation in our inversion procedure of both IR and UV observations in synergy should allow us to benefit from the complementary advantages of these various sensors. Unfortunately, such a synergy could not be achieved in this study. OMI observations of the volcanic SO₂ on 10 April 2011 could not be exploited here as they were largely hampered by the row anomaly, which has affected the quality of the Level 1B radiance data for a particular viewing direction since 2009. Furthermore, the Ozone Mapping and Profiler Suite (OMPS) sensor was not launched at the time of this eruption of Etna (Yang et al., 2013).

This study has shown that ground-based UV observations miss a large part of the SO₂ emitted by volcanoes during ash-rich eruptions. SO₂ flux is widely used in volcanology for tracking changes in the volcanic activity and providing crucial indications for eruption forecasting and hazard assessment (Sparks, 2003; Oppenheimer et al., 2011; Surono et al., 2012). At Etna, ground-based derived SO₂ emission rate was observed to drastically decrease, whereas the degassing and tremor seismicity were in reality escalating during the paroxysmal period of the activity (Fig. 3). Therefore, temporal variations of SO₂ flux delivered by ground UV-observations have to be treated with caution when degassing and volcanic activity intensify. We note that thermal observations, which are commonly used to monitor the volcanic activity as well, were also hampered by the abundance of ash within the plume (Bonaccorso et al., 2011).

These discrepancies between ground and spaceborne evaluations of SO₂ fluxes challenge our present estimates of the global degassing of sulfur compounds by volcanoes (Andres and Kasgnoc, 1998; Halmer et al., 2002), which may have been significantly under-estimated. Furthermore, the techniques for estimating the abundance of other major chemical compounds degassed by volcanoes (e.g. water, carbon dioxide (CO₂), hydrogen sulfide (H₂S), halogen halides (including HCl, HF, HBr, etc. . . .)) do not directly measure the flux of a specific species. These methods, either Fourier

vs satellite-based) can only be achieved by an estimation of a common parameter, such as the SO₂ flux emitted at the source. Our method of assimilation of SO₂ satellite observations using inversion schemes paves the way for the hybridization of ground and spaceborne SO₂ observations from various UV and IR sensors in a an automatic manner.

4.2 Strategy toward the assimilation of SO₂ cloud height imagery

By comparing the SO₂ cloud altitudes predicted by the inversion against altitudes derived from the analysis of IASI observations, we find a general agreement. This agreement is highlighted by the good linear regression with a slope near to unity in Fig. 10. Nevertheless, we may observe a scatter of the IASI altitudes that increases with model altitude. A systematic bias toward IASI altitudes most often larger than modeled ones may also be noticed.

These discrepancies stem from a combination of factors related to (1) SO₂ column amount (CA) and (2) background atmosphere:

1. Altitude information in the ν_3 band of SO₂ is derived mainly from the interference with water vapor absorption, which impacts the relative intensity of the difference SO₂ lines in the observed spectrum. Uncertainty on altitude increases with decreasing spectral signature (and therefore decreasing SO₂ CA or decreasing altitude). This explains in large part the scatter of IASI altitude values for low SO₂ CA. These are mostly found on the edges and in the tail of the volcanic cloud, as the column amount comes close to the detection threshold. A few isolated IASI pixels with abnormally low IASI altitudes, also very likely correspond to small SO₂ values (but inherent to the IR, assuming a too low altitude, artificially results in larger column estimates). These points correspond to an altitude of ~ 2 km according to the IASI retrieval, against 7–8 km in the model. They match the forefront of the volcanic SO₂ cloud in the 11 April p.m. image (Fig. 10), where the plume features a conspicuous discontinuity. These inconsistent values might also be related to

Temporal variations of flux and altitude of volcanic sulfur dioxide emissions

M. Boichu et al.

Title Page

Abstract

Introduction

Conclusions

References

Tables

Figures



Back

Close

Full Screen / Esc

Printer-friendly Version

Interactive Discussion



the presence of relatively thick meteorological clouds leading to an underestimation of the retrieved altitude (Fig. 4).

2. IASI retrievals were performed here using atmospheric parameters for the month of August 2011, over quite a large area around Etna, following a near-real-time processing strategy. Biases in this standard atmosphere, as compared to the actual atmosphere on 10–11 April, are likely to affect the retrieved altitude of a few kilometers and explain a large part of the positive bias toward larger IASI altitudes.

Due to the existence of the different sources of uncertainties listed above, the IASI-derived altitudes should be selected prior to the assimilation process. Indeed, biases affecting the retrieved altitudes would tend to map into biases in the inverted source history due to the trade-off between emission time and emission height resulting from wind shear. To circumvent these caveats, a selection of data characterized by a SO₂ load exceeding a certain threshold could be performed before their assimilation in the inversion procedure. Isolated IASI data co-located with a high value of the cloud cover factor could be also discarded for further analysis (Fig. 4).

This case study demonstrates the robustness of the altitude retrieval by both the model and IASI NRT products for monitoring SO₂ clouds of relatively weak intensity and altitude. Algorithms which exploit spaceborne hyperspectral UV observations generally require higher SO₂ loads for delivering an information on altitude (Yang et al., 2010; Nowlan et al., 2011; Rix et al., 2012).

Under favorable meteorological conditions, volcanic SO₂ clouds can be detected as well with spaceborne infrared sensors such as MODIS or SEVIRI (onboard the geostationary Meteosat Second Generation satellite). These instruments cannot provide quantitative estimates on the SO₂ abundance in the plume. However, as discussed in Sect. 3.2, the higher spatial (1 km × 1 km for MODIS IR channels and 250 m × 250 m for visible channels) or temporal (acquisitions at a specific location every ~ 15 min for SEVIRI) resolution of these observations in the near-source region provide crucial indications on the trajectory followed by the SO₂ plume in the vicinity of the source, as

Temporal variations of flux and altitude of volcanic sulfur dioxide emissions

M. Boichu et al.

Title Page

Abstract

Introduction

Conclusions

References

Tables

Figures



Back

Close

Full Screen / Esc

Printer-friendly Version

Interactive Discussion



illustrated by the animation using SEVIRI SO₂ acquisitions and MODIS SO₂ images for the Etna eruption on 10–11 April 2011 (Prata and Corradini, 2014). Consequently, such information could also be exploited and assimilated in an inversion procedure to better constrain the altitude of SO₂ emissions.

4.3 Strategy toward the assimilation of LiDAR observations

Images of SO₂ cloud height provided by infrared observations are generally not sensitive to SO₂ below 5 km. In a complementary manner, ground LiDAR measurements can deliver continuous information on the altitude of an aerosol-rich volcanic cloud passing over the station, the backscatter signal being of larger intensity for low altitude plumes. Although networks of ground-based LiDAR are growing, especially in Europe (Pappalardo et al., 2013; Haeffelin et al., 2012; Mortier et al., 2013), it will be a long time before large, remote geographical areas of the globe may be covered, such as above the sea or the ocean. For instance, the Etna SO₂ cloud mainly traveled above the Mediterranean Sea during the 2011 April eruption. In this context, spaceborne CALIOP LiDAR measurements, which are also more sensitive to high plumes, may capture a profile of the volcanic cloud. More broadly, LiDAR color and depolarization ratios allow for characterizing the microphysical properties of volcanic aerosols. Therefore, they provide the opportunity to gain a deeper understanding of the conversion of SO₂ to sulfate aerosols within volcanic clouds.

5 Conclusions and perspectives

This study demonstrates our capability to describe accurately the rapidly varying dynamics of volcanic SO₂ release with time, in terms of both emission rate and altitude, using inverse modeling procedures combining spaceborne imagery and chemistry-transport modeling.

Temporal variations of flux and altitude of volcanic sulfur dioxide emissions

M. Boichu et al.

Title Page

Abstract

Introduction

Conclusions

References

Tables

Figures

◀

▶

◀

▶

Back

Close

Full Screen / Esc

Printer-friendly Version

Interactive Discussion



Temporal variations of flux and altitude of volcanic sulfur dioxide emissions

M. Boichu et al.

Title Page

Abstract

Introduction

Conclusions

References

Tables

Figures



Back

Close

Full Screen / Esc

Printer-friendly Version

Interactive Discussion



SO₂ cloud, at large distance from the source, which are in agreement with recently developed products of SO₂ height retrieved from IASI observations, as well as with backward HYSPLIT trajectories. Second, spaceborne CALIOP LiDAR observations support the concomitant presence of sulfate aerosols alongside with the modeled volcanic SO₂ cloud at thousands of kilometers from the source.

These results confirm that both flux and altitude of SO₂ emissions are highly variable in time during an eruption. The characterization of these two emission parameters is consequently required to consistently describe the far-range dispersal of volcanic clouds. We have shown that specific wind shear conditions are required to derive the altitude of emissions simultaneously to the SO₂ flux if only SO₂ column amount maps are assimilated. Alternatively, the assimilation of the volcanic cloud altitude derived directly from hyperspectral imagery (e.g. IASI) should be considered as a promising strategy if these atmospheric conditions are not met. Nevertheless, as these observations would strongly constrain the altitude of emissions retrieved in the inversion procedure, care should be taken in accounting for the various factors affecting observed altitude values. In the specific case of IASI, such factors include the increasing uncertainty on the retrieved altitudes for low SO₂ column amounts, the sensitivity to the background atmospheric conditions used in the analysis, and the presence of thick meteorological clouds.

This study paves the way for a 4-D characterization of SO₂ cloud dispersal using hyperspectral spaceborne imagery through a combination of chemistry-transport modeling and radiative transfer modeling. As these spatial and temporal features of SO₂ clouds become accessible, vertically-resolved LiDAR observations should provide their full potential in bringing insights into the mechanisms of formation and degradation of volcanic sulfate aerosols.

Acknowledgements. M. Boichu gratefully acknowledges support from the Nord-Pas de Calais Regional Council for her junior research scientist fellowship and from the CaPPA (Chemical and Physical Properties of the Atmosphere) excellence laboratory. L. Clarisse is a Research Associate (Chercheur Qualifié) with F.R.S.-FNRS. He also gratefully acknowledges financial

support of ESA within the SACS2-SMASH project which allowed for performing the retrieval of the IASI dataset used in this study. The L1 and L2 CALIOP data, as well as the L1B radiances from MODIS/Aqua were obtained through the online archive of the ICARE (Cloud-Aerosol-Water-Radiation Interactions) Data and Services center (CNES, CNRS, Nord-Pas-De-Calais Regional Council, University of Lille, (<http://www.icare.univ-lille1.fr/>). M. Boichu warmly thanks N. Pascal (ICARE) for discussions and advices on CALIOP products and N. Ferlay (LOA) for providing a script for CALIOP data postprocessing. We gratefully acknowledge the NOAA Air Resources Laboratory for the provision of the HYSPLIT trajectory model and for their READY website used in this publication (<http://ready.arl.noaa.gov/HYSPLIT.php>).

References

- Alparone, S., Andronico, D., Lodato, L., and Sgroi, T.: Relationship between tremor and volcanic activity during the Southeast Crater eruption on Mount Etna in early 2000, *J. Geophys. Res.*, 108, 2241, doi:10.1029/2002JB001866, 2003. 5043
- Andres, R. and Kasgnoc, A.: A time-averaged inventory of subaerial volcanic sulfur emissions, *J. Geophys. Res.*, 103, 25251–25261, 1998. 5051
- Ansmann, A., Tesche, M., Seifert, P., Groß, S., Freudenthaler, V., Apituley, A., Wilson, K. M., Serikov, I., Linné, H., Heinold, B., Hiebsch, A., Schnell, F., Schmidt, J., Mattis, I., Wandinger, U., and Wiegner, M.: Ash and fine-mode particle mass profiles from EARLINET-AERONET observations over central Europe after the eruptions of the Eyjafjallajökull volcano in 2010, *J. Geophys. Res.*, 116, D00U02, doi:10.1029/2010JD015567, 2011. 5048
- Arellano, S. R., Hall, M., Samaniego, P., Le Pennec, J.-L., Ruiz, A., Molina, I., and Yepes, H.: Degassing patterns of Tungurahua volcano (Ecuador) during the 1999–2006 eruptive period, inferred from remote spectroscopic measurements of SO₂ emissions, *J. Volcanol. Geoth. Res.*, 176, 151–162, doi:10.1016/j.jvolgeores.2008.07.007, 2008. 5036, 5052
- August, T., Klaes, D., Schlüssel, P., Hultberg, T., Crapeau, M., Arriaga, A., O'Carroll, A., Coppens, D., Munro, R., and Calbet, X.: IASI on Metop-A: operational Level 2 retrievals after five years in orbit, *J. Quant. Spectrosc. Ra.*, 113, 1340–1371, 2012. 5042
- Bauduin, S., Clarisse, L., Clerbaux, C., Hurtmans, D., and Coheur, P.-F.: IASI observations of sulfur dioxide (SO₂) in the boundary layer of Norilsk, *J. Geophys. Res.*, 119, 4253–4263, doi:10.1002/2013JD021405, 2014. 5051

Temporal variations of flux and altitude of volcanic sulfur dioxide emissions

M. Boichu et al.

Title Page

Abstract

Introduction

Conclusions

References

Tables

Figures



Back

Close

Full Screen / Esc

Printer-friendly Version

Interactive Discussion



Temporal variations of flux and altitude of volcanic sulfur dioxide emissions

M. Boichu et al.

Title Page

Abstract

Introduction

Conclusions

References

Tables

Figures



Back

Close

Full Screen / Esc

Printer-friendly Version

Interactive Discussion



and May 2010, *Atmos. Chem. Phys.*, 12, 11417–11434, doi:10.5194/acp-12-11417-2012, 2012. 5036, 5038

Carn, S., Krueger, A., Arellano, S., Krotkov, N., and Yang, K.: Daily monitoring of Ecuadorian volcanic degassing from space, *J. Volcanol. Geoth. Res.*, 176, 141–150, doi:10.1016/j.jvolgeores.2008.01.029, 2008. 5050

Carn, S. A. and Bluth, G. J. S.: Prodigious sulfur dioxide emissions from Nyamuragira volcano, D. R. Congo, *Geophys. Res. Lett.*, 30, 2211, doi:10.1029/2003GL018465, 2003. 5035

Cashman, K., Sturtevant, B., Papale, P., and Navon, O.: Magmatic fragmentation, in: *Encyclopedia of Volcanoes*, edited by: Sigurdsson, H., Academic Press, San Diego, CA, 421–430, 2000. 5049

Clarisse, L., Hurtmans, D., Clerbaux, C., Hadji-Lazaro, J., Ngadi, Y., and Coheur, P.-F.: Retrieval of sulphur dioxide from the infrared atmospheric sounding interferometer (IASI), *Atmos. Meas. Tech.*, 5, 581–594, doi:10.5194/amt-5-581-2012, 2012. 5038, 5050

Clarisse, L., Coheur, P.-F., Theys, N., Hurtmans, D., and Clerbaux, C.: The 2011 Nabro eruption, a SO₂ plume height analysis using IASI measurements, *Atmos. Chem. Phys.*, 14, 3095–3111, doi:10.5194/acp-14-3095-2014, 2014. 5036, 5038, 5040, 5046

Clerbaux, C., Boynard, A., Clarisse, L., George, M., Hadji-Lazaro, J., Herbin, H., Hurtmans, D., Pommier, M., Razavi, A., Turquety, S., Wespes, C., and Coheur, P.-F.: Monitoring of atmospheric composition using the thermal infrared IASI/MetOp sounder, *Atmos. Chem. Phys.*, 9, 6041–6054, doi:10.5194/acp-9-6041-2009, 2009. 5038

Clerbaux, C. and Crevoisier, C.: New Directions: infrared remote sensing of the troposphere from satellite: less, but better, *Atmos. Environ.*, 72, 24–26, 2013. 5052

Delmelle, P.: Environmental impacts of tropospheric volcanic gas plumes, *Geol. Soc. Sp.*, 213, 381–400, 2003. 5034

Derimian, Y., Dubovik, O., Tanré, D., Goloub, P., Lapyonok, T., and Mortier, A.: Optical properties and radiative forcing of the Eyjafjallajökull volcanic ash layer observed over Lille, France, in 2010, *J. Geophys. Res.*, 117, D00U25, doi:10.1029/2011JD016815, 2012. 5048

Draxler, R. and Rolph, G.: HYSPLIT (HYbrid Single-Particle Lagrangian Integrated Trajectory) Model, Tech. Report, NOAA Air Resources Laboratory, Silver Spring, MD, available at: <http://ready.arl.noaa.gov/HYSPLIT.php> (last access: 18 February 2015), 2014. 5042

Dubuisson, P., Herbin, H., Minvielle, F., Compiègne, M., Thieuleux, F., Parol, F., and Pelon, J.: Remote sensing of volcanic ash plumes from thermal infrared: a case study analysis from

Temporal variations of flux and altitude of volcanic sulfur dioxide emissions

M. Boichu et al.

Title Page

Abstract

Introduction

Conclusions

References

Tables

Figures



Back

Close

Full Screen / Esc

Printer-friendly Version

Interactive Discussion



SEVIRI, MODIS and IASI instruments, *Atmos. Meas. Tech.*, 7, 359–371, doi:10.5194/amt-7-359-2014, 2014. 5041

Ebmeier, S. K., Sayer, A. M., Grainger, R. G., Mather, T. A., and Carboni, E.: Systematic satellite observations of the impact of aerosols from passive volcanic degassing on local cloud properties, *Atmos. Chem. Phys.*, 14, 10601–10618, doi:10.5194/acp-14-10601-2014, 2014. 5034

Eckhardt, S., Prata, A. J., Seibert, P., Stebel, K., and Stohl, A.: Estimation of the vertical profile of sulfur dioxide injection into the atmosphere by a volcanic eruption using satellite column measurements and inverse transport modeling, *Atmos. Chem. Phys.*, 8, 3881–3897, doi:10.5194/acp-8-3881-2008, 2008. 5035

Edmonds, M., Herd, R., Galle, B., and Oppenheimer, C.: Automated, high time-resolution measurements of SO₂ flux at Soufrière Hills Volcano, Montserrat, *B. Volcanol.*, 65, 578–586, 2003. 5036

Flemming, J. and Inness, A.: Volcanic sulfur dioxide plume forecasts based on UV satellite retrievals for the 2011 Grimsvötn and the 2010 Eyjafjallajökull eruption, *J. Geophys. Res.*, 118, 10172–10189, doi:10.1002/jgrd.50753, 2013. 5035

Freitas, S., Rodrigues, L. F., Longo, K. M., and Panetta, J.: Impact of a monotonic advection scheme with low numerical diffusion on transport modeling of emissions from biomass burning, *J. Adv. Model. Earth Syst.*, 4, M01001, doi:10.1029/2011MS000084, 2012. 5043

Galle, B., Johansson, M., Rivera, C., Zhang, Y., Kihlman, M., Kern, C., Lehmann, T., Platt, U., Arellano, S., and Hidalgo, S.: Network for Observation of Volcanic and Atmospheric Change (NOVAC), a global network for volcanic gas monitoring: network layout and instrument description, *J. Geophys. Res.*, 115, D05304, doi:10.1029/2009JD011823, 2010. 5036

Graf, H.-F., Feichter, J., and Langmann, B.: Volcanic sulfur emissions: estimates of source strength and its contribution to the global sulfate distribution, *J. Geophys. Res.*, 102, 10727–10738, 1997. 5034

Haefelin, M., Angelini, F., Morille, Y., Martucci, G., Frey, S., Gobbi, G., Lolli, S., O'Dowd, C., Sauvage, L., Xueref-Rémy, I., Wastine, B., and Feist, D.G.: Evaluation of mixing-height retrievals from automatic profiling lidars and ceilometers in view of future integrated networks in Europe, *Bound.-Lay. Meteorol.*, 143, 49–75, 2012. 5055

Halmer, M., Schminke, H.-U., and Graf, H.-F.: The annual volcanic gas input into the atmosphere, in particular into the stratosphere: a global data set for the past 100 years, *J. Volcanol. Geoth. Res.*, 115, 515–528, 2002. 5051

Temporal variations of flux and altitude of volcanic sulfur dioxide emissions

M. Boichu et al.

Title Page

Abstract

Introduction

Conclusions

References

Tables

Figures

◀

▶

◀

▶

Back

Close

Full Screen / Esc

Printer-friendly Version

Interactive Discussion



- Menut, L., Bessagnet, B., Khvorostyanov, D., Beekmann, M., Blond, N., Colette, A., Coll, I., Curci, G., Foret, G., Hodzic, A., Mailler, S., Meleux, F., Monge, J.-L., Pison, I., Siour, G., Turquety, S., Valari, M., Vautard, R., and Vivanco, M. G.: CHIMERE 2013: a model for regional atmospheric composition modelling, *Geosci. Model Dev.*, 6, 981–1028, doi:10.5194/gmd-6-981-2013, 2013. 5037
- Merucci, L., Burton, M., Corradini, S., and Salerno, G. G.: Reconstruction of SO₂ flux emission chronology from space-based measurements, *J. Volcanol. Geoth. Res.*, 206, 80–87, doi:10.1016/j.jvolgeores.2011.07.002, 2011. 5035, 5052
- Mortier, A., Goloub, P., Podvin, T., Deroo, C., Chaikovsky, A., Ajtai, N., Blarel, L., Tanre, D., and Derimian, Y.: Detection and characterization of volcanic ash plumes over Lille during the Eyjafjallajökull eruption, *Atmos. Chem. Phys.*, 13, 3705–3720, doi:10.5194/acp-13-3705-2013, 2013. 5055
- Moxnes, E., Kristiansen, N., Stohl, A., Clarisse, L., Durant, A., Weber, K., and Vogel, A.: Separation of ash and sulfur dioxide during the 2011 Grímsvötn eruption, *J. Geophys. Res.*, 119, 7477–7501, doi:10.1002/2013JD021129, 2014. 5035
- Neely, R., Toon, O., Solomon, S., Vernier, J.-P., Alvarez, C., English, J., Rosenlof, K., Mills, M., Bardeen, C., Daniel, J., and Thayer, J. P.: Recent anthropogenic increases in SO₂ from Asia have minimal impact on stratospheric aerosol, *Geophys. Res. Lett.*, 40, 999–1004, doi:10.1002/grl.50263, 2013. 5033
- Nowlan, C., Liu, X., Chance, K., Cai, Z., Kurosu, T., Lee, C., and Martin, R.: Retrievals of sulfur dioxide from the Global Ozone Monitoring Experiment 2 (GOME-2) using an optimal estimation approach: algorithm and initial validation, *J. Geophys. Res.*, 116, D18301, doi:10.1029/2011JD015808, 2011. 5036, 5054
- Oppenheimer, C.: Volcanic degassing, in: *Treatise on Geochemistry*, vol. 3, edited by: Rudnick, R. L., Holland, H. D., and Turekian, K. K., Elsevier, 123–166, doi:10.1016/B0-08-043751-6/03020-6, 2003. 5049
- Oppenheimer, C., Scaillet, B., and Martin, R. S.: Sulfur degassing from volcanoes: source conditions, surveillance, plume chemistry and earth system impacts, *Rev. Mineral. Geochem.*, 73, 363–421, doi:10.2138/rmg.2011.73.13, 2011. 5033, 5051
- Pappalardo, G., Mona, L., D'Amico, G., Wandinger, U., Adam, M., Amodeo, A., Ansmann, A., Apituley, A., Alados Arboledas, L., Balis, D., Boselli, A., Bravo-Aranda, J. A., Chaikovsky, A., Comeron, A., Cuesta, J., De Tomasi, F., Freudenthaler, V., Gausa, M., Giannakaki, E., Giehl, H., Giunta, A., Grigorov, I., Groß, S., Haeffelin, M., Hiebsch, A., Iarlori, M., Lange, D.,

**Temporal variations
of flux and altitude of
volcanic sulfur
dioxide emissions**

M. Boichu et al.

Title Page

Abstract

Introduction

Conclusions

References

Tables

Figures



Back

Close

Full Screen / Esc

Printer-friendly Version

Interactive Discussion

Linné, H., Madonna, F., Mattis, I., Mamouri, R.-E., McAuliffe, M. A. P., Mitev, V., Molero, F., Navas-Guzman, F., Nicolae, D., Papayannis, A., Perrone, M. R., Pietras, C., Pietruczuk, A., Pisani, G., Preißler, J., Pujadas, M., Rizi, V., Ruth, A. A., Schmidt, J., Schnell, F., Seifert, P., Serikov, I., Sicard, M., Simeonov, V., Spinelli, N., Stebel, K., Tesche, M., Trickl, T., Wang, X., Wagner, F., Wiegner, M., and Wilson, K. M.: Four-dimensional distribution of the 2010 Eyjafjallajökull volcanic cloud over Europe observed by EARLINET, *Atmos. Chem. Phys.*, 13, 4429–4450, doi:10.5194/acp-13-4429-2013, 2013. 5048, 5055

Petersen, G. N., Bjornsson, H., and Arason, P.: The impact of the atmosphere on the Eyjafjallajökull 2010 eruption plume, *J. Geophys. Res.*, 117, D00U07, doi:10.1029/2011JD016762, 2012. 5034

Prata, A.: Satellite detection of hazardous volcanic clouds and the risk to global air traffic, *Nat. Hazards*, 51, 303–324, doi:10.1007/s11069-008-9273-z, 2009. 5041

Prata, F. and Corradini, S.: SEVIRI SO₂ animation and MODIS SO₂ images for the eruption of Etna on 10–11 April 2011, available at: <http://savaa.nilu.no/Etna.aspx> (last access: 18 December 2014), 2014. 5055

Pyle, D. and Mather, T.: Halogens in igneous processes and their fluxes to the atmosphere and oceans from volcanic activity: a review., *Chem. Geol.*, 263, 110–121, doi:10.1016/j.chemgeo.2008.11.013, 2009. 5052

Rix, M., Valks, P., Hao, N., Loyola, D., Schlager, H., Huntrieser, H., Flemming, J., Koehler, U., Schumann, U., and Inness, A.: Volcanic SO₂, BrO and plume height estimations using GOME-2 satellite measurements during the eruption of Eyjafjallajökull in May 2010, *J. Geophys. Res. Atmos.*, 117, D00U19, doi:10.1029/2011JD016718, 2012. 5036, 5054

Robock, A.: Volcanic eruptions and climate, *Rev. Geophys.*, 38, 191–220, doi:10.1029/1998RG000054, 2000. 5033

Salerno, G. G., Burton, M. R., Oppenheimer, C., Caltabiano, T., Randazzo, D., Bruno, N., and Longo, V.: Three-years of SO₂ flux measurements of Mt. Etna using an automated UV scanner array: comparison with conventional traverses and uncertainties in flux retrieval, *J. Volcanol. Geoth. Res.*, 183, 76–83, doi:10.1016/j.jvolgeores.2009.02.013, 2009. 5039

Santer, B., Painter, J., Mears, C., Doutriaux, C., Caldwell, P., Arblaster, J., Cameron-Smith, P., Gillett, N., Gleckler, P., Lanzante, J., Perlwitz, J., Solomon, S., Stott, P. A., Taylor, K. E., Terray, L., Thorne, P. W., Wehner, M. F., Wentz, F. J., Wigley, T. M. L., Wilcox, L. J., and Zou, C.: Identifying human influences on atmospheric temperature, *P. Natl. Acad. Sci. USA*, 110, 26–33, 2013. 5033

**Temporal variations
of flux and altitude of
volcanic sulfur
dioxide emissions**

M. Boichu et al.

Title Page

Abstract

Introduction

Conclusions

References

Tables

Figures



Back

Close

Full Screen / Esc

Printer-friendly Version

Interactive Discussion

- Santer, B. D., Bonfils, C., Painter, J. F., Zelinka, M. D., Mears, C., Solomon, S., Schmidt, G. A.,
Fyfe, J. C., Cole, J. N., Nazarenko, L., Taylor, K. E., and Wentz, F. J.: Volcanic contribution to
decadal changes in tropospheric temperature, *Nat. Geosci.*, 7, 185–189, 2014. 5033
- Sassen, K.: Polarization in Lidar, Springer, New York, 2005. 5048
- 5 Sassen, K. and Benson, S.: A midlatitude cirrus cloud climatology from the facility for atmo-
spheric remote sensing. Part II: Microphysical properties derived from lidar depolarization, *J.*
Atmos. Sci., 58, 2103–2112, 2001. 5048
- Sassen, K., Zhao, H., and Yu, B.-K.: Backscatter laser depolarization studies of simulated
stratospheric aerosols: crystallized sulfuric acid droplets, *Appl. Optics*, 28, 3024–3029, 1989.
10 5049
- Schmidt, A., Carslaw, K. S., Mann, G. W., Rap, A., Pringle, K. J., Spracklen, D. V., Wilson, M.,
and Forster, P. M.: Importance of tropospheric volcanic aerosol for indirect radiative forcing of
climate, *Atmos. Chem. Phys.*, 12, 7321–7339, doi:10.5194/acp-12-7321-2012, 2012. 5034
- Skamarock, J., Klemp, W., Dudhia, J., Gill, D., Barker, D., Duda, M., Huang, X., Wang, W., and
15 Powers, J.: A description of the advanced research WRF version 3, NCAR technical note,
NCAR/TN-475+ STR, doi:10.5065/D68S4MVH, 2008. 5037
- Solomon, S.: Stratospheric ozone depletion: a review of concepts and history, *Rev. Geophys.*,
37, 275–316, 1999. 5033
- Solomon, S., Daniel, J., Neely, R., Vernier, J.-P., Dutton, E., and Thomason, L.: The persistently
20 variable background stratospheric aerosol layer and global climate change, *Science*, 333,
866–870, 2011. 5033
- Sparks, R.: Forecasting volcanic eruptions, *Earth Planet. Sc. Lett.*, 210, 1–15, 2003. 5051
- Sparks, R., Bursik, M., Carey, S., Gilbert, J., Glaze, L., Sigurdsson, H., and Woods, A.: *Volcanic
Plumes*, John Wiley and Sons, New-York, 1997. 5045
- 25 Spinei, E., Carn, S. A., Krotkov, N. A., Mount, G. H., Yang, K., and Krueger, A.: Validation of
ozone monitoring instrument SO₂ measurements in the Okmok volcanic cloud over Pullman,
WA, July 2008, *J. Geophys. Res.*, 115, D00L08, doi:10.1029/2009JD013492, 2010. 5052
- Stevenson, D., Johnson, C., Collins, W., and Derwent, R.: The tropospheric sulphur cycle and
the role of volcanic SO₂, *Geol. Soc. Sp.*, 213, 295–305, 2003. 5033, 5034
- 30 Stohl, A., Prata, A. J., Eckhardt, S., Clarisse, L., Durant, A., Henne, S., Kristiansen, N. I.,
Minikin, A., Schumann, U., Seibert, P., Stebel, K., Thomas, H. E., Thorsteinsson, T.,
Tørseth, K., and Weinzierl, B.: Determination of time- and height-resolved volcanic ash emis-

Temporal variations of flux and altitude of volcanic sulfur dioxide emissions

M. Boichu et al.

Title Page

Abstract

Introduction

Conclusions

References

Tables

Figures



Back

Close

Full Screen / Esc

Printer-friendly Version

Interactive Discussion



- sions and their use for quantitative ash dispersion modeling: the 2010 Eyjafjallajökull eruption, *Atmos. Chem. Phys.*, 11, 4333–4351, doi:10.5194/acp-11-4333-2011, 2011. 5034
- Surono, Jousset, P., Pallister, J., Boichu, M., Buongiorno, M. F., Budisantoso, A., Costa, F., Andreastuti, S., Prata, F., Schneider, D., Clarisse, L., Humaida, H., Sumarti, S., Bignami, C., Griswold, J., Carn, S., Oppenheimer, C., and Lavigne, F.: The 2010 explosive eruption of Java's Merapi volcano – a “100-year” event, *J. Volcanol. Geoth. Res.*, 241–242, 121–135, doi:10.1016/j.jvolgeores.2012.06.018, 2012. 5035, 5049, 5050, 5051
- Tamburello, G., Aiuppa, A., Kanzas, E., McGonigle, A., and Ripepe, M.: Passive vs. active degassing modes at an open-vent volcano (Stromboli, Italy), *Earth Planet. Sc. Lett.*, 359, 106–116, 2012. 5052
- Theys, N., Champion, R., Clarisse, L., Brenot, H., van Gent, J., Dils, B., Corradini, S., Merucci, L., Coheur, P.-F., Van Roozendaal, M., Hurtmans, D., Clerbaux, C., Tait, S., and Ferrucci, F.: Volcanic SO₂ fluxes derived from satellite data: a survey using OMI, GOME-2, IASI and MODIS, *Atmos. Chem. Phys.*, 13, 5945–5968, doi:10.5194/acp-13-5945-2013, 2013. 5035
- Thordarson, T. and Self, S.: Atmospheric and environmental effects of the 1783–1784 Laki eruption: a review and reassessment, *J. Geophys. Res.*, 108, 4011, doi:10.1029/2001JD002042, 2003. 5034
- Vaughan, M. A., Young, S. A., Winker, D. M., Powell, K. A., Omar, A. H., Liu, Z., Hu, Y., and Hostetler, C. A.: Fully automated analysis of space-based lidar data: an overview of the CALIPSO retrieval algorithms and data products, *Proc. SPIE 5575, Laser Radar Techniques for Atmospheric Sensing*, 16, doi:10.1117/12.572024, 2004. 5048
- Vernier, J.-P., Thomason, L. W., Pommereau, J.-P., Bourassa, A., Pelon, J., Garnier, A., Hauchecorne, A., Blanot, L., Treppe, C., Degenstein, D., and Vargas, F.: Major influence of tropical volcanic eruptions on the stratospheric aerosol layer during the last decade, *Geophys. Res. Lett.*, 38, 12807, doi:10.1029/2011GL047563, 2011. 5033, 5041, 5047
- Watson, I., Realmuto, V., Rose, W., Prata, A., Bluth, G., Gu, Y., Bader, C., and Yu, T.: Thermal infrared remote sensing of volcanic emissions using the moderate resolution imaging spectroradiometer, *J. Volcanol. Geoth. Res.*, 135, 75–89, 2004. 5041
- Winker, D. M., Liu, Z., Omar, A., Tackett, J., and Fairlie, D.: CALIOP observations of the transport of ash from the Eyjafjallajökull volcano in April 2010, *J. Geophys. Res.*, 117, D00U15, doi:10.1029/2011JD016499, 2012. 5041, 5047, 5048
- Yang, K., Liu, X., Bhartia, P. K., Krotkov, N. A., Carn, S. A., Hughes, E. J., Krueger, A. J., Spurr, R. J., and Trahan, S. G.: Direct retrieval of sulfur dioxide amount and altitude from

**Temporal variations
of flux and altitude of
volcanic sulfur
dioxide emissions**

M. Boichu et al.

Title Page

Abstract

Introduction

Conclusions

References

Tables

Figures



Back

Close

Full Screen / Esc

Printer-friendly Version

Interactive Discussion



spaceborne hyperspectral UV measurements: theory and application, J. Geophys. Res., 115, D00L09, doi:10.1029/2010JD013982, 2010. 5036, 5054

Yang, K., Dickerson, R. R., Carn, S. A., Ge, C., and Wang, J.: First observations of SO₂ from the satellite Suomi NPP OMPS: widespread air pollution events over China, Geophys. Res. Lett., 40, 4957–4962, 2013. 5051

Yuan, T., Remer, L. A., and Yu, H.: Microphysical, macrophysical and radiative signatures of volcanic aerosols in trade wind cumulus observed by the A-Train, Atmos. Chem. Phys., 11, 7119–7132, doi:10.5194/acp-11-7119-2011, 2011. 5034

Zakšek, K., Hort, M., Zaletelj, J., and Langmann, B.: Monitoring volcanic ash cloud top height through simultaneous retrieval of optical data from polar orbiting and geostationary satellites, Atmos. Chem. Phys., 13, 2589–2606, doi:10.5194/acp-13-2589-2013, 2013. 5041

Temporal variations of flux and altitude of volcanic sulfur dioxide emissions

M. Boichu et al.

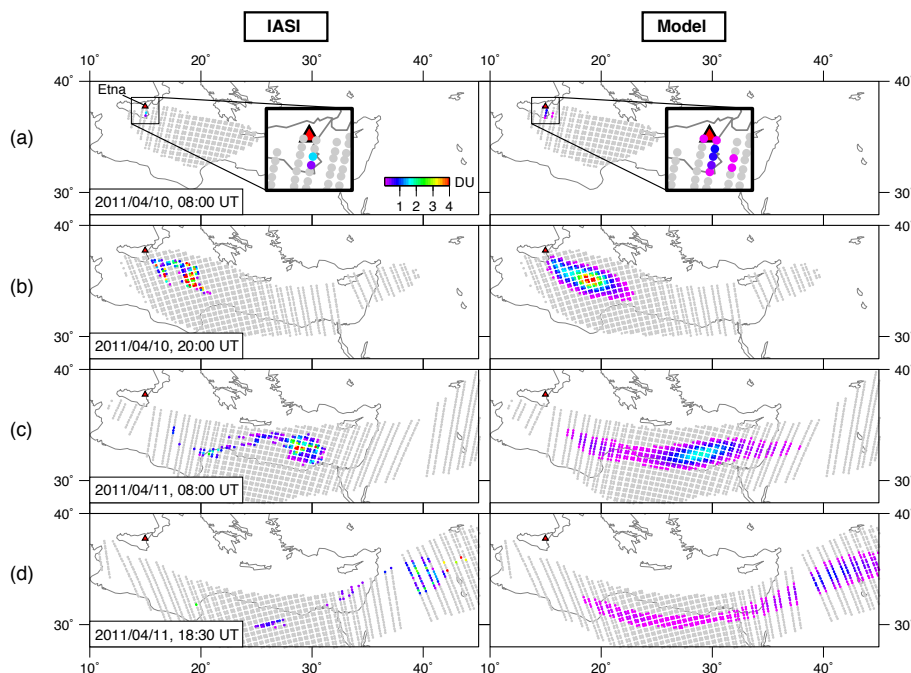


Figure 2. Maps of SO_2 column amounts (DU) in the Etna volcanic cloud on 10 and 11 April 2011 (left) retrieved from IASI observations acquired over a time window centered at the date indicated, and (right) simulated with the CHIMERE chemistry-transport model initialized with emissions reconstructed by the inversion procedure. Regions in grey indicate column amounts < 0.1 DU.

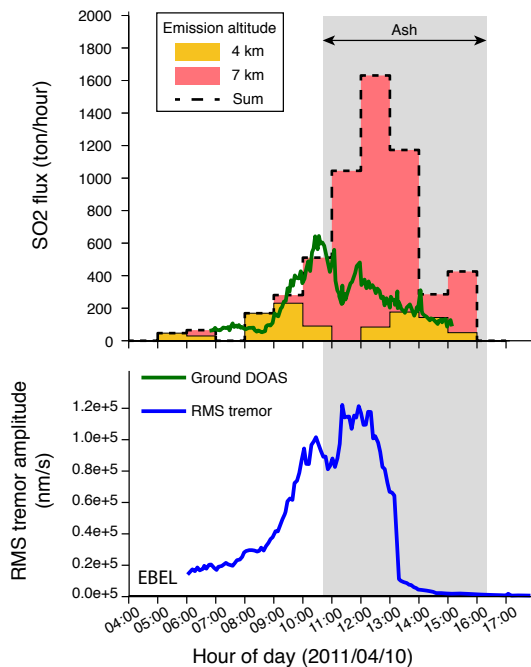


Figure 3. Etna emissions during the 10 April 2011 eruption. (Top) Temporal evolution of the SO_2 flux (th^{-1}) measured from ground-based UV-DOAS observations during daylight hours (from Bonaccorso et al., 2011) (green line) and retrieved using the inversion procedure which assimilated IASI SO_2 column amount observations (histograms). Yellow and pink areas indicate the proportion of the flux emitted at respectively 4 and 7 km a.s.l. The dashed envelope corresponds to the total flux. The grey zone indicates presence of ash (Bonaccorso et al., 2011). (Bottom) Root mean square amplitude of the seismic tremor (0.5–5 Hz) recorded at the station the closest to the South-East Crater where the eruption takes place (from Bonaccorso et al., 2011).

Temporal variations of flux and altitude of volcanic sulfur dioxide emissions

M. Boichu et al.

Title Page

Abstract Introduction

Conclusions References

Tables Figures

◀ ▶

◀ ▶

Back Close

Full Screen / Esc

Printer-friendly Version

Interactive Discussion



Temporal variations of flux and altitude of volcanic sulfur dioxide emissions

M. Boichu et al.

Title Page

Abstract

Introduction

Conclusions

References

Tables

Figures



Back

Close

Full Screen / Esc

Printer-friendly Version

Interactive Discussion

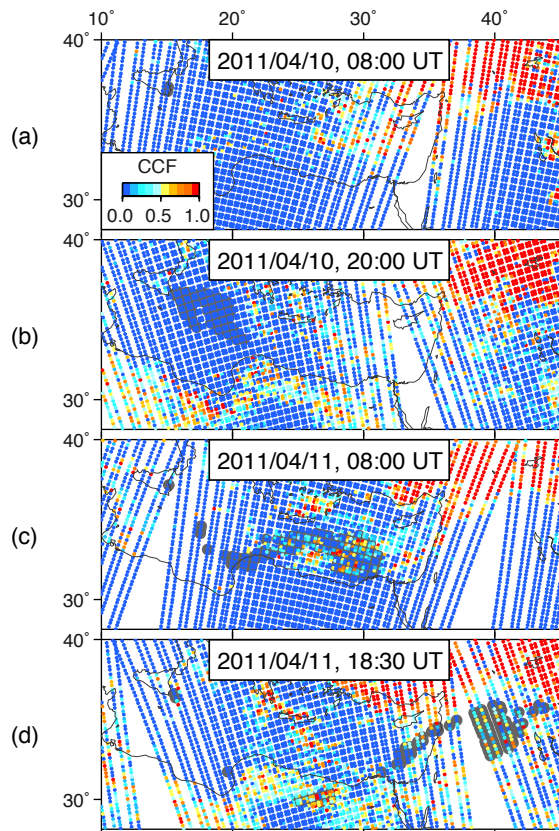


Figure 4. Maps of the cloud cover factor (CCF). The Etna IASI SO₂ cloud is shown in grey in the background.

Temporal variations of flux and altitude of volcanic sulfur dioxide emissions

M. Boichu et al.

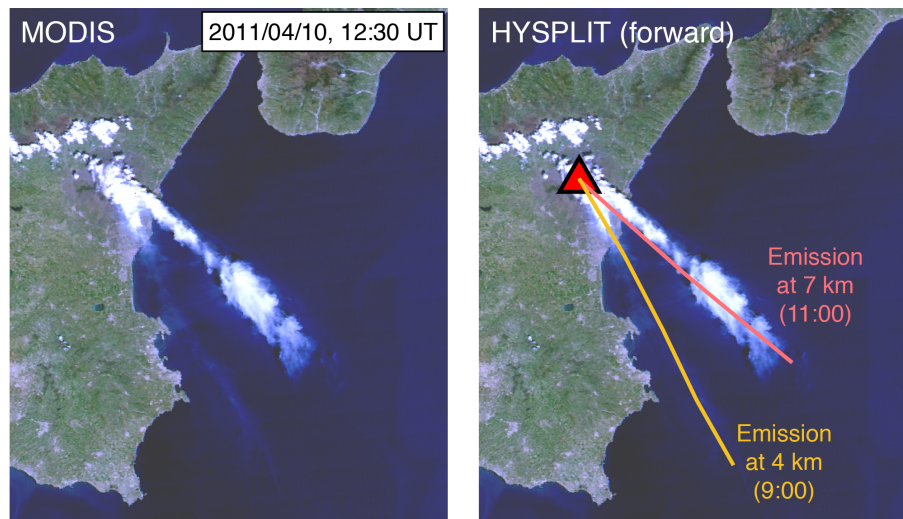


Figure 5. (Left) MODIS/AQUA RGB image of Etna plumes on 10 April 2011 at 12:30 UT obtained from visible channels. (Right) Same as left panel, overlaid with the forward trajectories from the Lagrangian HYSPLIT model initialized with (yellow line) an emission at 4 km a.s.l. starting at 09:00 UT and (pink line) an emission at 7 km a.s.l. starting at 11:00 UT in agreement with the modeled source term with the inversion procedure (same color code as in Fig. 3). Trajectories are computed until 13:00 UT.

Title Page

Abstract

Introduction

Conclusions

References

Tables

Figures

◀

▶

◀

▶

Back

Close

Full Screen / Esc

Printer-friendly Version

Interactive Discussion



Temporal variations of flux and altitude of volcanic sulfur dioxide emissions

M. Boichu et al.

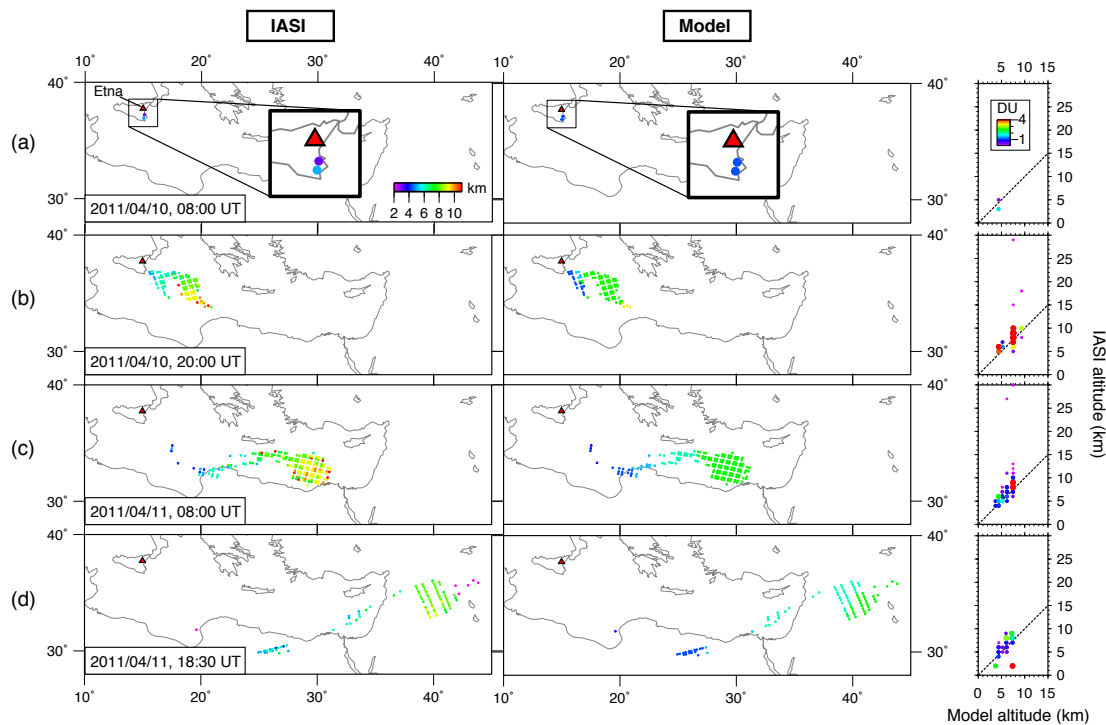


Figure 6. Maps of the altitude (km a.s.l.) of the Etna SO_2 cloud on 10 and 11 April 2011 (left) retrieved from IASI observations and (middle) predicted by the forward CHIMERE chemistry-transport model initialized with emissions reconstructed from the inversion procedure (Fig. 3). (Right) Scatter plot of IASI altitudes with modeled altitudes. Symbol color and size depend on observed IASI SO_2 column amount (DU).

Temporal variations of flux and altitude of volcanic sulfur dioxide emissions

M. Boichu et al.

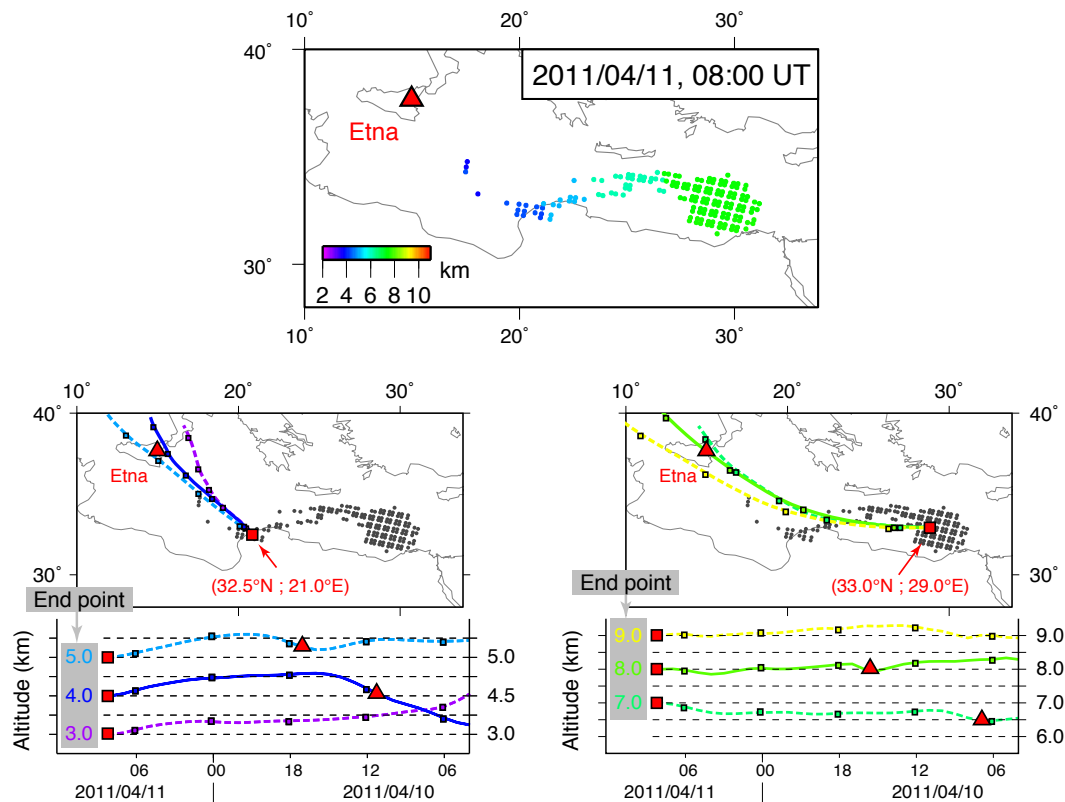


Figure 7. Comparison of the altitude (km a.s.l.) of the dispersed Etna SO₂ cloud on 11 April 2011 08:00 UT (top) simulated with the CHIMERE chemistry-transport model, initialized with emissions reconstructed by the inversion procedure and (bottom) deduced from HYSPLIT backward trajectories starting from two opposite extremities of the SO₂ cloud either above Lybia (32.5° N, 21.0° E) (bottom left) or offshore Egypt (33.0° N, 29.0° E) (bottom right).

Title Page

Abstract

Introduction

Conclusions

References

Tables

Figures

◀

▶

◀

▶

Back

Close

Full Screen / Esc

Printer-friendly Version

Interactive Discussion



Temporal variations
of flux and altitude of
volcanic sulfur
dioxide emissions

M. Boichu et al.

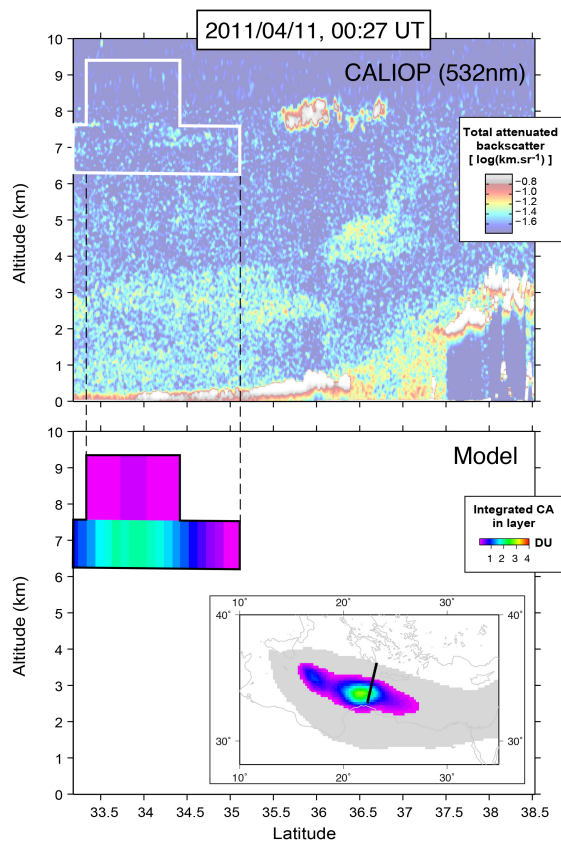


Figure 8. CALIOP track crossing the Etna volcanic cloud on 11 April 2011 00:27 UT. (Top) CALIOP total attenuated backscatter signal at 532 nm. (Bottom) Cross-section and dispersion map of the modeled SO₂ cloud at the time and location of the CALIOP track.

Temporal variations of flux and altitude of volcanic sulfur dioxide emissions

M. Boichu et al.

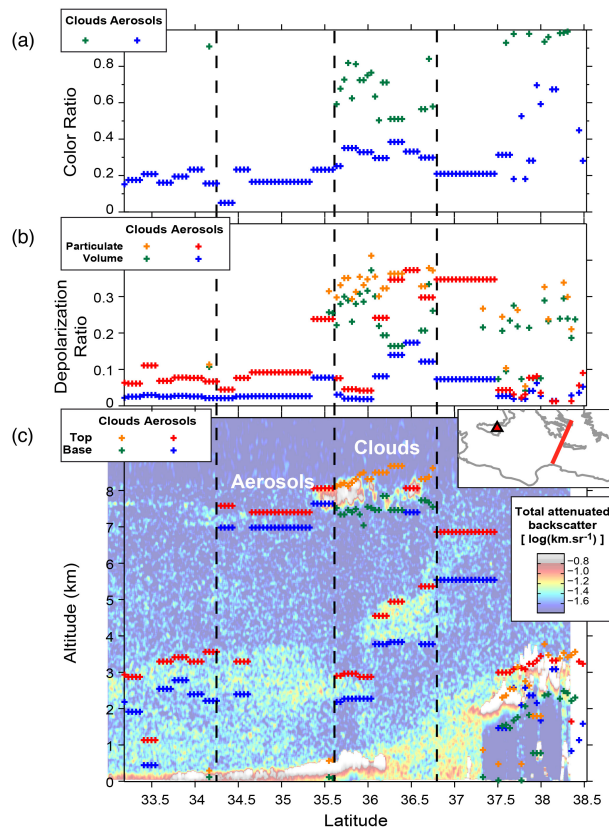


Figure 9. CALIOP track crossing the Etna volcanic cloud on 11 April 2011 00:27 UT. (Bottom) Altitude (top and base) of the highest layer of aerosols (blue, red) or meteorological clouds (green, orange) retrieved from Level 2 CALIOP analysis is superimposed on the total attenuated backscatter signal at 532 nm. (Middle) Volume and particulate depolarization ratios for aerosols (blue, red) or clouds (green, orange). (Top) Total color ratio for aerosols (blue) or clouds (green).

[Title Page](#)
[Abstract](#)
[Introduction](#)
[Conclusions](#)
[References](#)
[Tables](#)
[Figures](#)
[◀](#)
[▶](#)
[◀](#)
[▶](#)
[Back](#)
[Close](#)
[Full Screen / Esc](#)
[Printer-friendly Version](#)
[Interactive Discussion](#)

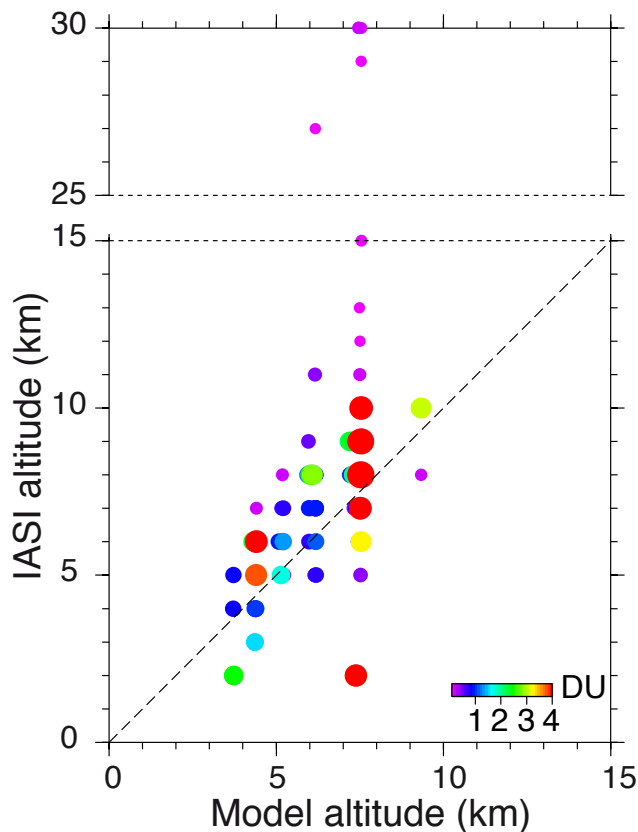


Figure 10. Scatter plot of the altitude of the Etna SO₂ cloud retrieved from IASI observations with the modeled altitude predicted with the CHIMERE model initialized with emissions reconstructed from the inversion of IASI SO₂ column amounts (DU). All data from 10 April a.m. to 11 April p.m. 2011 are included. Symbol color and size depend on IASI SO₂ column amount (DU). Note the change of scale in the Y axis at an altitude > 15 km.

Temporal variations of flux and altitude of volcanic sulfur dioxide emissions

M. Boichu et al.

Title Page

Abstract

Introduction

Conclusions

References

Tables

Figures

◀

▶

◀

▶

Back

Close

Full Screen / Esc

Printer-friendly Version

Interactive Discussion

